Electronic structure and transport properties of CrAs/GaAs/CrAs trilayers from first principles theory

O. Bengone,[1,2] O. Eriksson,[1] J. Fransson,[1,3] I. Turek,[4,5] J. Kudrnovský,[6,7,8] and V. Drchal[6,7]
[1]*Department of Physics, Uppsala University, Box 530, SE-75121, Uppsala, Sweden*
[2]*Department of Physical Electronic/Photonic, Mitthögskolan, Sundsvall, Sweden*
[3]*Department of Materials Science and Engineering, Royal Institute of Technology (KTH), SE-100 44 Stockholm, Sweden*
[4]*Institute of Physics of Materials, Academy of Sciences of the Czech Republic, Žižkova 22, CZ-616 62 Brno, Czech Republic*
[5]*Department of Electronic Structure, Charles University, Ke Karlovu 5, CZ-12116 Prague 2, Czech Republic*
[6]*Institute of Physics, Academy of Sciences of the Czech Republic, Na Slovance 2, CZ-182 21 Prague 8, Czech Republic*
[7]*Center for Computational Materials Science, Technical University of Vienna, Getreidemarkt 9/158, A-1060 Vienna, Austria*
[8]*Max-Planck-Institut für Mikrostrukturphysik, Weinberg 2, D-06120 Halle, Germany*
(Received 18 February 2004; published 9 July 2004)

We present a theoretical study of the transport properties of a CrAs/GaAs/CrAs trilayer. The theory was based on a first principles method for calculating the electronic structure, in combination with a Kubo-Landauer approach for calculating the transport properties in a current perpendicular to the plane geometry. We have also investigated the electronic structure and the magnetic properties of this trilayer, with special focus on electronic and magnetic properties at the CrAs/GaAs interface. Finally, we have studied the effects of chemical disorder on the transport properties, in particular the influence of As antisites at both the Cr and Ga sites.

DOI: 10.1103/PhysRevB.70.035302 PACS number(s): 75.47.De, 72.10.−d, 72.15.Gd

I. INTRODUCTION

The increased interest in the magnetic and transport properties of thin film systems is mainly caused by the complexity and challenging academic questions these man-made materials raise, in combination with the potential use of such systems in sensor applications.[1] A large number of multilayers have been fabricated and their magnetic and transport properties have been studied. Novel effects, such as the interlayer exchange coupling[2] and the giant magnetic resistance (GMR) effect[3–5] have been discovered experimentally and analyzed theoretically.[6–10]

Of particular interest are the half-metallic ferromagnets (HMF), i.e., compounds for which only one spin direction has a gap at the Fermi level E_F, while the other has metallic character. This class of ferromagnets, first predicted by de Groot *et al.*[11] based on band structure calculations for $C1_b$ type Heusler alloys, are now intensively studied because they should provide a current with a high degree of spin polarization and improve significantly the performance of magneto-optical devices such as tunneling magnetoresistance devices. Recently, Akinaga *et al.*[12] have found that metastable *zinc-blende* type CrAs grown on GaAs(001) substrate exhibits well-pronounced HMF character, but the most prominent feature is its high Curie temperature above 400°K. In fact, a large number of artificial *zinc-blende* transition metal compounds exhibit HMF character, and some of them, e.g., MnAs or CrAs, have already been grown on different substrates.[13–16]

Based on first-principles calculations, Galanakis and Mavropoulos[17,18] have investigated the half-metallic character of 3*d* transition metal pnictides and chalcogenides for different lattice constants, simulating the growth of these compounds on different substrates. Also, Sanyal *et al.*[19], Xie *et al.*,[20,21] and Shirai[22] have investigated the magnetic properties, half metallicity, and structural stability of several promising pnictide- and chalcogenide-based materials. Pask *et al.*[23] have investigated the stability of *zinc-blende* Mn and Cr pnictides and carbides and suggested appropriate substrates for their growth. Kübler,[24] Sakuma,[25] and Kudrnovský *et al.*[26] have calculated the exchange interaction and found a high Curie temperature for *zinc-blende* type CrAs and similar compounds.

However, the relation between transport properties and magnetism has not been addressed with equal intensity. The magnetoresistance of a MnAs/GaAs/MnAs trilayer heterostructure has been studied and a small magnetoresistance ratio less than 1% has been measured for a current-in-plane (CIP) geometry. Transport properties of digital ferromagnetic heterostructure MnAs/GaAs have been calculated by Sanvito and Hill[27] and they found a high spin-polarized tunneling current close to 100% for the current-perpendicular to plane (CPP) geometry and a large metallic conductance in MnAs in the CIP geometry. Also, Pampuch *et al.*[28] have suggested that α-MnAs film on GaAs(001) substrate could be used as a magnetologic gate.

We have chosen here to investigate the CrAs/GaAs/CrAs trilayer with special emphasis on the transport properties. In this paper we have also studied the electronic structure and magnetism of the CrAs/GaAs/CrAs trilayer. We have also investigated the effects of As antisites defects at Ga or Cr sites and how they affects the electronic structure, magnetism, and most importantly the transport properties.

The paper is organized as follows. In Sec. II we present the method used to resolve the electronic structure and the transport properties, and we describe the computational details of the system. In Sec. III we describe the electronic structure and the transport properties of the ideal CrAs/GaAs/CrAs trilayer without defects. In Sec. IV we analyze the effect of chemical disorder. Finally we summarize our results in Sec. V.

0163-1829/2004/70(3)/035302(6)/$22.50 ©2004 The American Physical Society

II. METHOD OF CALCULATION

The electronic structure of the system is described in terms of a surface Green's function technique implemented within the framework of a tight-binding linear muffin-tin orbital approach.[29] This approach allows us to simulate on an *ab initio* level the experimental conditions in the CPP configuration with two semi-infinite leads sandwiching the active region composed of alternated magnetic and nonmagnetic layers.

The corresponding transport properties are evaluated within a Kubo-Landauer approach in the CPP geometry, based on a transmission matrix formulation within the linear response theory (see Ref. 31). Recently, the theory has been adapted and implemented for general crystallographic orientations of atomic layers.[32] In this approach the conductance of the system is given by

$$C^{\sigma}(E_F) = \frac{e^2}{h}\frac{1}{N_{\parallel}}\sum_{\mathbf{k}_{\parallel}} T^{\sigma}_{\mathbf{k}\parallel}(E_F) = \frac{e^2}{h}\frac{1}{N_{\parallel}}\sum_{\mathbf{k}_{\parallel}} \mathrm{tr}\{B^{\sigma}_{L} g^{\sigma+}_{1,N} B^{\sigma}_{R} g^{\sigma-}_{N,1}\}_{\mathbf{k}_{\parallel}}, \tag{1}$$

where σ is the spin index ($\sigma=\uparrow,\downarrow$) and e^2/h is the quantum conductance. B^{σ}_{L} (B^{σ}_{R}) is the anti-Hermitian part of the so-called embedding potential describing the influence of the left (right) semi-infinite lead onto the N-layers active region. The quantity $g^{\sigma+}_{1,N}(g^{\sigma-}_{N,1})$ is the off-diagonal retarded (advanced) Green's function matrix, linking the left lead and the right lead.[29] The trace over angular momenta and sites in the unit cell is denoted by tr. The conductance is then obtained by summing the transmission probability $T^{\sigma}_{\mathbf{k}_{\parallel}}(E_F)$ of each channel $\mathbf{k}_{\parallel}$ in the surface Brillouin zone (SBZ).

This approach can be extended to systems with chemical disorder such as interface interdiffusion and/or alloyed layers, within a lateral two-dimensional supercell method[31,33] with random occupation of supercell lattice sites by atoms A and B, corresponding to the layerwise alloy composition $A_{1-x}B_x$. The transmission coefficients for the supercell can then be decomposed as a sum of a ballistic part, with scattering between states with the same $\mathbf{k}_{\parallel}$ vector of the original (1×1)-cell SBZ, and a diffusive part, with scattering between different $\mathbf{k}_{\parallel}$ and $\mathbf{k}_{\parallel}'$ states in the original SBZ.[34] With this supercell technique, our description allows us to study disordered systems and it treats ballistic and diffusive scattering on equal footing on a quantitative level.

The electronic structure was determined self-consistently within the local spin density approximation, with Vosko-Wilk-Nusair parameterization for the exchange-correlation potential.[30] We used a $4s^24p^1$ and $4s^24p^3$ valence configuration for Ga atoms and As atoms, respectively, with the filled $3d$ shell treated as the core, while Cr atoms are described by a $3d^54s^1$ valence configuration. The calculations were carried out with a 256 $\mathbf{k}_{\parallel}$ points mesh in the original (1×1)-cell SBZ. For disordered systems, the potentials are determined self-consistently using the coherent potential approximation (CPA).[29] The potentials determined for a given alloy composition were used in transport calculations for various random supercell configurations, neglecting therefore fluctuations of the potentials due to variations of the local environment. For all transport calculations, ideal and disordered systems, we used 10^4 $\mathbf{k}_{\parallel}$ points in the original SBZ. For disordered systems, an average conductance over four alloy configurations is evaluated in a (4×4) two-dimensional lateral supercell. A small imaginary part $\delta=10^{-7}$ Ry has been added to the energy in order to evaluate the Green's function quantities entering in the conductance calculation.

The system studied consists of a trilayer nCrAs/mGaAs/nCrAs, grown in the *zinc-blende* structure (001 direction), embedded in two semi-infinite leads. We have used the principal layer technique with two atomic layers per principal layer, one Cr (or Ga) layer and one As layer. In the two-dimensional cell, each atomic layer is composed of two atomic sites, one containing a Cr (or Ga) atom together with an empty sphere, and one containing an As atom together with an empty sphere. The empty spaces were included only to obtain a closer packing of atomic spheres in the *zinc-blende* structure. We used the same Wigner-Seitz radius $r_{\mathrm{ASA}}=2.6294$ a.u. for all atomic components in the trilayer structure, which corresponds to a lattice constant of GaAs ($a_{\mathrm{GaAs}}=5.65$ Å). In a Landauer formulation, one needs to include leads that act as electron reservoirs. In our study we choose vanadium as the lead material because it is paramagnetic and has an in-plane lattice constant that allows matching with the CrAs (and GaAs) structure. At the interface between CrAs and the lead, we found that a V/As interface (As-terminated CrAs) is preferable in order to keep a Cr environment that renders half-metallicity. For a Cr-terminated interface, the hybridization between Cr and V affects the Cr magnetic moment substantially, and hence also the half metallic properties of the CrAs layers. Hence in our study we used As terminated layers at the CrAs/V interface.

III. IDEAL LAYERS WITHOUT DEFECTS

In the *zinc-blende* structure with T_d^2 as the space group, the Cr atoms have tetrahedral environment with As atoms at the tetrahedron corners. Due to this tetrahedral symmetry, the d states split in a lower doubly degenerate e level ($d_{3z^2-r^2}$ and $d_{x^2-y^2}$ orbitals) and a higher triply degenerate level (d_{xy}, d_{xz}, and d_{yz} orbitals) with t_2 symmetry. Within the tetrahedral symmetry, $p-d$ mixing is allowed and the d states of Cr with t_2 symmetry can hybridize with the As p states also with t_2 symmetry.[35,36] This induces a large bonding-antibonding splitting that opens up a gap.

The e states ($d_{3z^2-r^2}$ and $d_{x^2-y^2}$) belong to a different irreducible representation, with different symmetry and therefore do not hybridize with As p states. Consequently, these states become nonbonding and lie in the gap caused by the p-d hybridization of Cr and As t_2 states. In addition, the exchange splitting shifts the relative position of the two majority and minority spin channels, and the Fermi level lies in the band gap for the minority spin, and in the antibonding band for the majority spin, resulting in a half-metallic compound. To illustrate this we show in Fig. 1 the atom-resolved density of states (DOS) of bulk CrAs in the *zinc-blende* structure for the GaAs lattice constant. We also show in Fig. 1(b) the t_2- and e-decomposed DOS for the Cr atoms.

In Fig. 2 we present the atom-resolved DOS for some selected bilayers (Cr,As or Ga,As) in the

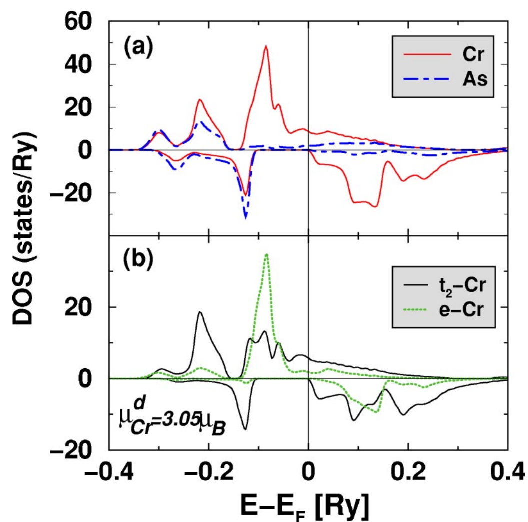

FIG. 1. (Color online) Calculated DOS of bulk CrAs in the *zinc-blende* structure for the GaAs lattice constant (a_{GaAs}=5.65 Å). In (a) we show the Cr and As projected states and in (b) we show the Cr projected states onto e and t_2 symmetry. The vertical line denotes the Fermi energy.

5CrAs/5GaAs/5CrAs trilayer. Bilayers on the CrAs side are denoted IA-2, IA-1, and IA, respectively, when approaching the CrAs/GaAs interface from the CrAs side, and on the GaAs side they are denoted IB+2, IB+1 and IB from the GaAs side. (With this notation, the bilayers CrAs IA-2 and GaAs IB+2 correspond to the center of the 5CrAs layers and the 5GaAs layers, respectively.) We observe that deep in the layer (IA-2 for CrAs and IB+2 for GaAs), the DOS looks like the corresponding bulk DOS with well-defined half-metallic character for CrAs and a well-defined band gap for GaAs. As one approaches the CrAs/GaAs interface, the DOS is modified. For instance, for CrAs the gap in the minority spin channel is much narrower, and there is only a pseudo-gap. Also, the peak just below −0.1 Ry in the minority spin channel is less pronounced both for the As and Cr atoms. The

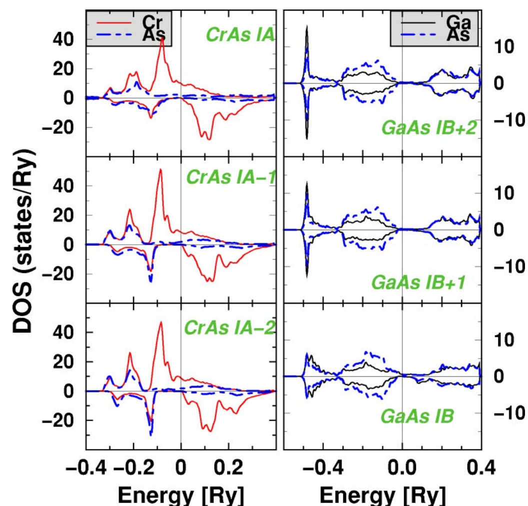

FIG. 2. (Color online) Calculated DOS of selected CrAs layers of the 5CrAs/5GaAs/5CrAs trilayer. The vertical lines denote the Fermi energy.

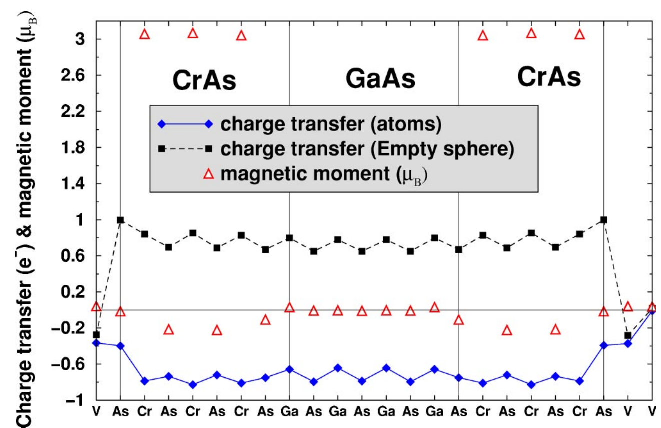

FIG. 3. (Color online) Charge transfer and magnetic moments in the 3CrAs/4GaAs/3CrAs trilayer for the ferromagnetic coupling of the two CrAs magnetic layers.

reduced intensity and broadening of this structure reveals a decrease of the Cr-As t_2 hybridization, therefore a decrease of the bonding-antibonding splitting responsible for the gap. We also note that around the same energy (−0.1 Ry) but for majority spin states, the small gap separating the two structures (bonding t_2 and nonbonding from e) disappears as one moves towards the interface.

On the GaAs side, the most striking change is the closure of the band gap (GaAs IB) and a wider bandwidth for the states around −0.5 Ry. We also note a small polarization of GaAs states due to proximity effects with the spin-polarized Cr states. However, a small but nonzero band gap subsists in the minority spin channel that turns out to give a GaAs layer at the interface that is half-metallic.

It is well known that the LSDA underestimates the size of the band gap in semiconductors (due to overestimation of delocalization and hybridization by the use of information taken from the homogeneous electron-gas). Hence it is relevant to ask how reliably we can reproduce finer details concerning the band gap and half-metallicity of the presently studied systems (and similar systems). With a better theoretical description of the band gap (like GW, exact exchange, or other approximation), we expect that the majority spin channel of the GaAs layer in proximity to CrAs will keep its band gap, which will result in a higher effective barrier of tunneling from the CrAs layer.

Since the electronic structure of the CrAs and GaAs layers for the interface-2 and interface-1 layers is very similar to that of bulk CrAs and GaAs, respectively, we conclude that the changes in the electronic structure are dominated by changes in the nearest-neighboring environment. Hence one may, for convenience, calculate the electronic structure of the CrAs/GaAs/CrAs trilayer using somewhat reduced thicknesses for the CrAs layers. We have done so and used a 3CrAs/4GaAs/3CrAs trilayer. However one has to bear in mind that transport properties do depend on the thicknesses. The magnetic moment (triangle) for each atom site in the 3CrAs/4GaAs/3CrAs trilayer, in a ferromagnetic configuration, is shown in Fig. 3. Deep in the CrAs layer, Cr and As atoms exhibit a total magnetic moment of 3.09μ_B and −0.22μ_B, respectively. These moments become somewhat re-

TABLE I. Spin-resolved conductances per layer atom (in units e^2/h) calculated for a 3CrAs/mGaAs/3CrAs trilayer sandwiched by two semi-infinite leads (m is the number of GaAs layers). The subscripts F and AF denote the ferromagnetic or antiferromagnetic coupling of the two magnetic slabs.

	$C_F^{\uparrow}$	$C_F^{\downarrow}$	$C_{AF}^{\uparrow}$	$C_{AF}^{\downarrow}$
3CrAs/4GaAs	0.01797	9×10^{-8}	3×10^{-5}	3×10^{-5}
3CrAs/5GaAs	0.00677	2×10^{-8}	1×10^{-5}	1×10^{-5}
3CrAs/6GaAs	0.00398	1×10^{-8}	6×10^{-6}	6×10^{-6}
3CrAs/8GaAs	0.000430	$<10^{-8}$	7×10^{-7}	9×10^{-7}
3CrAs/10GaAs	0.000121	$<10^{-8}$	1×10^{-7}	1×10^{-7}
5CrAs/4GaAs	0.01008	$<10^{-8}$	3×10^{-5}	3×10^{-5}

duced to $3.06\mu_B$ and $-0.11\mu_B$ at the GaAs interface, i.e., the moments of the interface atoms are very similar to the moments deep in the films. For the empty spheres we found a nonzero magnetic moment of $+0.12\mu_B$ (not shown) only for empty sphere sites in the same atomic plane as the As atom in the CrAs layer.

The charge transfer for each site of the 3CrAs/4GaAs/3CrAs trilayer is also shown in Fig. 3. In the CrAs layer, we observe a charge transfer, compared to free atoms, with a decrease of –0.8 and –0.7 electrons for Cr and As atoms, respectively. Correspondingly, the empty spheres show an excess of electrons of +0.85 and +0.69 for sites in the Cr atomic plane and the As atomic plane, respectively. In the GaAs layer, Ga atoms show a decrease of –0.65 electrons while the decrease is of –0.7 electrons for the As atoms. Figure 3 shows that the charge transfer is essentially the same for the GaAs region and the CrAs region.

In Table I, we show the conductance (in e^2/h units) for the ideal 3CrAs/mGaAs/3CrAs trilayer (without defects) as a function of insulator thickness (m=4, 5, 6, 8, and 10). For comparison we also present the calculated conductance for a 5CrAs/4GaAs/5CrAs trilayer, and we note that qualitatively this trilayer behaves similar to the 3CrAs/4GaAs/3CrAs trilayer. Overall, one may note from the table that for all the studied trilayers the conductance is nonzero only for the spin-up channel of the parallel configuration ($C_F^{\uparrow}$) of the two CrAs layer magnetizations, which is due to the half-metallic character of the CrAs layers. For the antiferromagnetic coupling between CrAs layers across the GaAs layer we calculate a vanishingly small conductance, which would result in a large tunneling magnetoresistance (TMR). Note that because of the geometry of the system with one vanadium layer on one side and two vanadium layers one the other side of the active region, the system are not rigorously symmetric (see abscissa of Fig. 3). As a consequence, conductances for the AF configuration is not exactly identical for the spin-up and spin-down channels. From the table it is also clear that the conductance for the ferromagnetic configuration decreases as the insulator thickness increases, due to a larger width of the barrier. The decrease is highly nonlinear and reflects the expected exponential decay of the transmission as the barrier width increases. This fact is further illustrated in Fig. 4, where the data from the first principles calculations (diamonds) have been fitted with the conductance of a

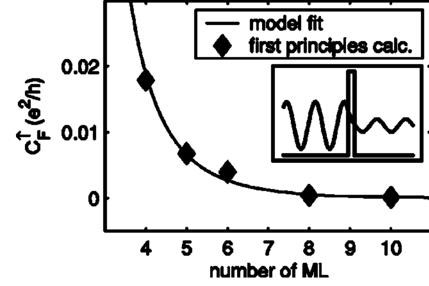

FIG. 4. Model fit (solid line) of the spin-up conductance ($C_F^{\uparrow}$) obtained from the first principles calculation (diamonds). The effective mass $m^*=0.02m_e$ has been used in the insulator region of length L. In the inset we show the geometry of the model potential and the wave function.

rectangular-shaped tunnel barrier (solid line). The transmission coefficient used for this calculation is given by

$$T(E) = \frac{1}{1+\left(\frac{k^2+\kappa^2}{2k\kappa}\right)^2 \sinh^2\kappa L}, \quad E < E_F,$$

$$k = \sqrt{2mE/\hbar^2},$$

$$\kappa = \sqrt{2m^*(V_0 - E)/\hbar^2}. \tag{2}$$

Here, m^* is the electron effective mass in the insulator region of length L, whereas V_0 is the barrier height relative to the Fermi energy. For large L, the transmission coefficient $T(E)\sim[4k\kappa/(k^2+\kappa^2)]^2\exp(-2\kappa L)$, which shows the exponential decay of $T(E)$ as a function of the insulator thickness L. The fitted conductance is obtained by summing the transmission coefficient in Eq. (2) up to the Fermi energy, in order to include in our one-dimensional model, the projected $\mathbf{k}_{\parallel}$-components of the states. The model fit reproduces all

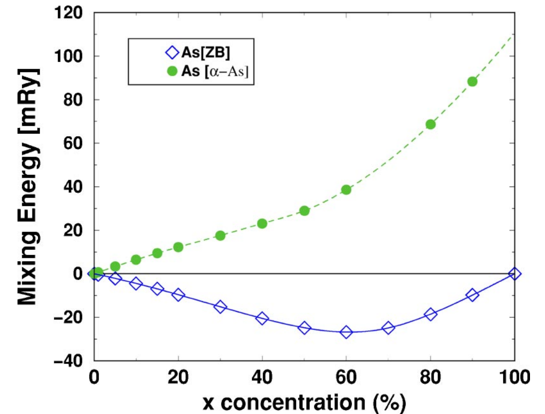

FIG. 5. Mixing energy of As antisites in $(Cr_{1-x}As_x)As$ structure. The energy of the As phase has been computed for the *zinc-blende* structure (with lattice parameter of CrAs, a_0=5.65 Å) as well as for the ground-state trigonal structure (α-As) for the experimental equilibrium volume V=21.3 Å^3 per atom. Lines are guide for the eyes.

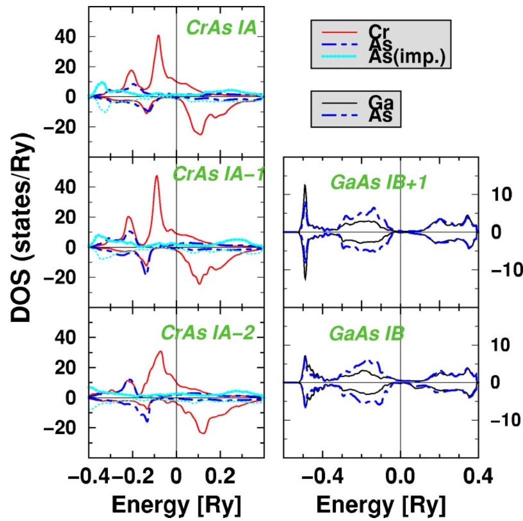

FIG. 6. (Color online) Calculated DOS of CrAs layers in the 3CrAs/4GaAs/3CrAs trilayer with 12.5% As_{Cr} antisites. The vertical lines denote the Fermi energy.

values of the conductance within reasonable limits, as can be seen in Fig. 4.

IV. EFFECT OF DISORDER

Due to high equilibrium vapor pressure of As, epitaxial growth of CrAs is usually performed at a certain As overpressure that produces As-rich CrAs. Since a production of CrAs/GaAs/CrAs trilayers is expected not to be possible without defects we have calculated the transport properties as a function of As antisites, both on the Cr and Ga sites. Before we report the results of this calculation, we first consider the stability of the system with As antisites. Hence we show in Fig. 5 the calculated mixing energy, i.e., the calculated energy difference $E[(Cr_{(1-x)}As_x)As]-x\,E[AsAs]-(1-x)E[CrAs]$, where $E[AsAs]$ is either in the metastable *zinc-blende* or the ground-state trigonal structure, all other phases are in the *zinc-blende* structure. Note that for As with one atom constituent, the *zinc-blende* structure is equivalent to the diamond structure. It is important to note that the ground-state of solid phase As is not the diamond structure but instead a trigonal structure (α-As),[37–39] therefore, *zinc-blende* As corresponds to a metastable phase. However, CrAs in the *zinc-blende* structure is also a metastable phase that is stabilized as overlayers on *zinc-blende* GaAs.

From the figure, one can conclude that phase separation of *zinc-blende* CrAs and trigonal As (α-As) is preferable compared to the alloy, in the case of the As-rich system (circles). On the other hand, $(Cr_{1-x}As_x)As$ alloy with As_{Cr} antisites is likely to happen if the *zinc-blende* structure is preserved, also for the As phase (diamonds). Due to the stabilizing mechanism produced by a *zinc-blende* substrate or GaAs layers, it is not unlikely that excess As atoms are situated on a *zinc-blende* lattice. For this reason, we have investigated also the effect of As_{Cr} antisites on the transport properties.

TABLE II. Spin-resolved conductances per layer atom (in units e^2/h) calculated for 3CrAs/4GaAs/3CrAs trilayer with 12.5% As antisites at Cr sites and 4% As antisites at Ga sites.

	$C_F^{\uparrow}$	$C_F^{\downarrow}$	$C_{AF}^{\uparrow}$	$C_{AF}^{\downarrow}$
As_{Ga}	0.017886	0.000186	0.000246	0.000398
As_{Cr}	0.010827	0.000580	0.004148	0.002940

In Fig. 6, the atom projected DOS is shown for 12.5% of As antisites at Cr sites. One may see that it affects the conducting properties since a small metallic character is developed in the CrAs layers (e.g., the CrAs IA-2 layer). However, for the CrAs layers close to the GaAs interface there is still a half metallic character in the DOS. Table II shows the calculated conductance for a CrAs/GaAs/CrAs trilayer with 12.5% As antisites at Cr sites and 4% As antisites at Ga sites. Although the presence of defects in the GaAs and CrAs layers slightly increases the conductance of the AF coupling, compared to the data in Table I, we nevertheless predict a very large magnetoresistive effect, since the AF coupling gives a substantially smaller conductance than the ferromagnetic coupling.

V. CONCLUSION

We have studied the electronic structure and conductance of CrAs/GaAs/CrAs trilayers using a first principles technique. Both the presence of defects (As antisites) and defect-free trilayers have been considered. We predict that a large magnetoresistance effect should be observed, for the antiferromagnetic alignment of the CrAs layers exhibits a vanishingly low conductance (even in the presence of As antisite defects). In addition, we found a large spin-polarization of the current in the case of ferromagnetic orientation of the magnetic (CrAs) slabs. We have analyzed our calculations with a simple square-well model potential and an analytical expression for the transmission coefficient. The simple model reproduces the numerical data rather well. Finally, we have investigated the stability of As antisites in CrAs and found that in the case of As-rich content, the antisites should be present if the *zinc-blende* structure is preserved, although a phase separation between *zinc-blende* CrAs and trigonal As cannot be excluded.

ACKNOWLEDGMENTS

This work was supported by the Computational Magnetoelectronics (HPRN-CT-2000-00143) RTN network of the European Commission. O.B. and O.E. are grateful to the Strategic Foundation for Research (SSF), the Swedish Research Council (VR), and to the Göran Gustafsson foundation for support. I.T., J. K., and V.D. acknowledge support of the Grant Agency of the Czech Republic (No. 202/04/0583).

[1] G. A. Prinz, Science **282**, 1660 (1998).
[2] P. Grünberg, R. Schreiber, Y. Pang, M. B. Brodsky, and H. Sowers, Phys. Rev. Lett. **57**, 2442 (1986).
[3] M. N. Baibich, J. M. Broto, A. Fert, F. Nguyen Van Dau, F. Petroff, P. Etienne, G. Creuzet, A. Friederich, and J. Chazelas Phys. Rev. Lett. **61**, 2472 (1988).
[4] G. Binasch, P. Grünberg, F. Saurenbach, and W. Zinn, Phys. Rev. B **39**, 4828 (1989).
[5] S. S. P. Parkin, R. Bhadra, and K. P. Roche, Phys. Rev. Lett. **66**, 2152 (1991).
[6] P. Bruno and C. Chappert, Phys. Rev. Lett. **67**, 1602 (1991).
[7] M. van Schilfgaarde, F. Herman, S. S. P. Parkin, and J. Kudrnovský, Phys. Rev. Lett. **74**, 4063 (1995).
[8] L. Nordström, P. Lang, R. Zeller, and P. H. Dederichs, Europhys. Lett. **29**, 395 (1994).
[9] T. Valet and A. Fert, Phys. Rev. B **48**, 7099 (1993).
[10] W. H. Butler, X-G. Zhang, D. M. C. Nicholson, and J. M. MacLaren, J. Magn. Magn. Mater. **151**, 354 (1995).
[11] R. A. de Groot, F. M. Mueller, P. G. van Engen, and K. H. J. Buschow, Phys. Rev. Lett. **50**, 2024 (1983).
[12] H. Akinaga, T. Manago, and M. Shirai, Jpn. J. Appl. Phys., Part 2 **39**, L1118 (2000).
[13] K. Takahashi and M. Tanaka, J. Appl. Phys. **87**, 6695 (2000).
[14] V. H. Etgens, M. Eddrief, D. H. Mosca, M. Marangolo, and J. M. George, J. Magn. Magn. Mater. **226–230**, 1577 (2001).
[15] V. H. Etgens, M. Eddrief, D. Demaille, Y. L. Zheng, and A. Ouerghi, J. Magn. Magn. Mater. **240**, 64 (2001).
[16] M. Mizuguchi, H. Akinaga, T. Manago, K. Ono, M. Oshima, M. Shirai, M. Yuri, H. J. Lin, H. H. Hsieh, and T. Chen, J. Appl. Phys. **91**, 7917 (2002).
[17] I. Galanakis and P. Mavropoulos, Phys. Rev. B **67**, 104417 (2003).
[18] I. Galanakis Phys. Rev. B **66**, 012406 (2002).
[19] B. Sanyal, L. Bergqvist, and O. Eriksson, Phys. Rev. B **68**, 054417 (2003).
[20] W.-H. Xie, Y.-Q. Xu, B.-G. Liu, and D. G. Pettifor, Phys. Rev. Lett. **91**, 037204 (2003); **91**, 219901(E) (2003).
[21] W.-H. Xie, B.-G. Liu, and D. G. Pettifor, Phys. Rev. B **68**, 134407 (2003).
[22] M. Shirai, J. Appl. Phys. **93**, 6844 (2003).
[23] J. E. Pask, L. H. Yang, C. Y. Fong, W. E. Pickett, and S. Dag, Phys. Rev. B **67**, 224420 (2003).
[24] J. Kübler, Phys. Rev. B **67**, 220403 (2003).
[25] A. Sakuma, J. Phys. Soc. Jpn. **71**, 2534 (2002).
[26] J. Kudrnovský, I. Turek, V. Drchal, F. Máca, P. Weinberger, and P. Bruno, Phys. Rev. B **69**, 115208 (2004).
[27] S. Sanvito and N. A. Hill, Phys. Rev. Lett. **87**, 267202 (2001).
[28] C. Pampuch, A. K. Das, A. Ney, L. Däweritz, R. Koch, and K. H. Ploog, Phys. Rev. Lett. **91**, 147203 (2003).
[29] I. Turek, V. Drchal, J. Kudrnovský, M. Šob, and P. Weinberger, *Electronic Structure of Disordered Alloys, Surfaces and Interfaces* (Kluwer, Dordrecht, 1997).
[30] S. H. Vosko, L. Wilk, and M. Nusair, Can. J. Phys. **58**, 1200 (1980).
[31] J. Kudrnovský, V. Drchal, C. Blaas, P. Weinberger, I. Turek, and P. Bruno, Phys. Rev. B **62**, 15084 (2000).
[32] O. Bengone, O. Eriksson, S. Mirbt, I. Turek, V. Drchal, and J. Kudrnovský, Phys. Rev. B **69**, 092406 (2004).
[33] P. Bruno, H. Itoh, J. Inoue, and S. Nomoyama, J. Magn. Magn. Mater. **198–199**, 46 (1999).
[34] V. Drchal, J. Kudrnovský, P. Bruno, P. H. Dederichs, I. Turek, and P. Weinberger, Phys. Rev. B **65**, 214414 (2002).
[35] S-H. Wei and Alex Zunger, Phys. Rev. B **37**, 8958 (1988).
[36] R. H. Parmenter, Phys. Rev. **100**, 573 (1955).
[37] R. J. Needs, R. M. Martin, and O. H. Nielsen, Phys. Rev. B **33**, 3778 (1986).
[38] L. F. Mattheiss, D. R. Hamann, and W. Weber, Phys. Rev. B **34**, 2190 (1986).
[39] K. Seifert, J. Hafner, J. Furthmüller, and G. Kresse, J. Phys.: Condens. Matter **7**, 3683 (1995).